Lena Maier-Hein, Conor J. Walsh, Alexander Seitel, Nevan C. Hanumara, Jo-Anne Shepard, A. M. Franz, F. Pianka, Sascha A. Müller, Bruno Schmied, Alexander H. Slocum, Rajiv Gupta, and Hans-Peter Meinzer, "Human vs. robot operator error in a needle-based navigation system for percutaneous liver interventions," Medical Imaging 2009: Visualization, Image-Guided Procedures, and Modeling, Michael I. Miga, Kenneth H. Wong, Editors, Proc. SPIE 7261, 72610X (2009).

http://dx.doi.org/10.1117/12.811334

Human vs. robot operator error in a needle-based navigation system for percutaneous liver interventions

Lena Maier-Hein[a], Conor J. Walsh[b], Alexander Seitel[a], Nevan C. Hanumara[b], Jo-Anne Shepard[c], A. M. Franz[a], F. Pianka[d], Sascha A. Müller[d], Bruno Schmied[d], Alexander H. Slocum[b], Rajiv Gupta[c], and Hans-Peter Meinzer[a]

[a]German Cancer Research Center, Div. of Medical and Biological Informatics,
[b]Massachusetts Institute of Technology, Dept. of Mechanical Engineering,
[c]Massachusetts General Hospital, Dept. of Radiology
[d]University of Heidelberg, Dept. of General, Abdominal and Transplant Surgery

ABSTRACT

Computed tomography (CT) guided percutaneous punctures of the liver for cancer diagnosis and therapy (e.g. tumor biopsy, radiofrequency ablation) are well-established procedures in clinical routine. One of the main challenges related to these interventions is the accurate placement of the needle within the lesion. Several navigation concepts have been introduced to compensate for organ shift and deformation in real-time, yet, the operator error remains an important factor influencing the overall accuracy of the developed systems. The aim of this study was to investigate whether the operator error and, thus, the overall insertion error of an existing navigation system could be further reduced by replacing the user with the medical robot Robopsy. For this purpose, we performed navigated needle insertions in a static abdominal phantom as well as in a respiratory liver motion simulator and compared the human operator error with the targeting error performed by the robot. According to the results, the Robopsy driven needle insertion system is able to more accurately align the needle and insert it along its axis compared to a human operator. Integration of the robot into the current navigation system could thus improve targeting accuracy in clinical use.

Keywords: Robotic Surgery, Image-Guided Therapy, Abdominal Procedures

1. PURPOSE

Computed tomography (CT) guided percutaneous punctures of the liver for cancer diagnosis and therapy (e.g. tumor biopsy, radiofrequency ablation) are well-established procedures in clinical routine.[1–3] One of the main challenges related to these interventions is the accurate placement of the needle within the lesion because the liver is subject to respiratory motion.[2,4] To address this issue, several navigation systems have been introduced which can guide the physician towards a preselected target (e.g.[5–13]). The overall insertion error of these systems typically comprises (cf. Fig. 2)

1. the **system error**, which includes the instrument tracking error and the target registration error (TRE), and
2. the **operator error** which reflects how accurately the operator can transfer a trajectory to the patient based on a given visualization scheme.

In previous reports,[14–17] we introduced a needle-based navigation concept for CT-guided punctures of the liver. It uses a real-time deformation model to continuously estimate the position of an initially determined target structure from a set of optically tracked fiducial needles. In our latest animal study, we obtained a mean overall insertion error of 3.7 ± 2.3 mm, which included an operator error of 2.4 ± 2.1 mm ($n = 32$).[16] The aim

Further author information:
Lena Maier-Hein: E-mail: l.maier-hein@dkfz-heidelberg.de, Telephone: +49 (0)6221 42-2341
Conor J. Walsh: E-mail: walshcj@mit.edu, Telephone: +1 617 780-9915

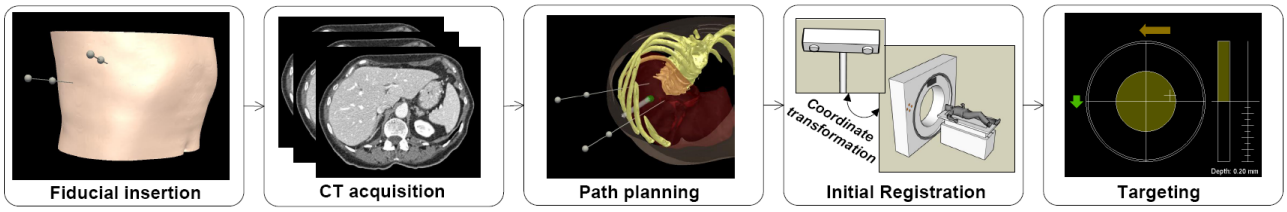

Figure 1. Workflow for navigated needle placement. First, the fiducial needles are inserted in the vicinity of the target. Next, a planning computed tomography (CT) scan is acquired which is used to plan a trajectory to the target. Finally, the image coordinate system is registered with the tracking coordinate system. During the intervention, a real-time deformation model is used to continuously estimate the position of the target point from the current positions of the optically tracked fiducial needles, and a navigation display (Fig. 3) supports the targeting process accordingly.

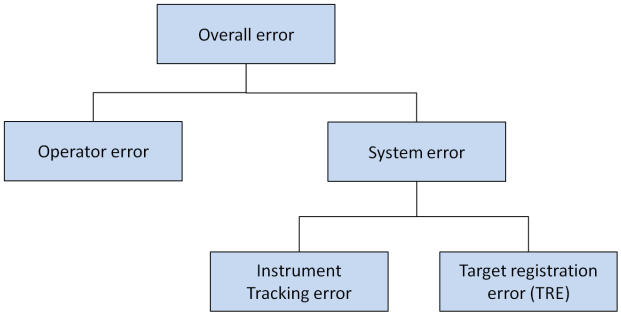

Figure 2. Sources of error contributing to the overall needle insertion error associated with the proposed navigation approach (cf. Fig. 1).

of this study is to investigate whether the operator error and thus the overall insertion error could be further reduced by replacing the user with a medical robot for the needle orientation and insertion. For this purpose, we perform navigated needle insertions both in a static phantom and in a respiratory liver motion simulator and compare the human operator error with the targeting error performed by the medical robot Robopsy.

2. MATERIALS AND METHODS

This section introduces the navigation system (section 2.1), the Robopsy system (section 2.2), the phantoms applied in this study (section 2.3) and the experiments performed to compare the robot error with the human operator error (section 2.4).

2.1 Needle-based navigation system

The navigation system was developed with the open-source cross-platform library *The Medical Imaging Interaction Toolkit* (MITK)[18] and was introduced in detail in previous reports.[14–17] It uses a real-time deformation model to continuously estimate the position of an initially determined target structure from a set of percutaneously inserted fiducial needles. The workflow is shown in Fig. 1. To transfer a planned trajectory accurately to the patient, we developed a three-stage visualization system which guides the user to the target (Fig. 3):

Tip positioning: The image generated in the first step is meant to assist the physician in finding the predetermined entry point with the tip of the instrument. For this purpose, the tip of the instrument is projected onto a plane perpendicular to the planned trajectory as shown in Fig. 3(a). The physician then has to move the tip of the needle essentially parallel to the skin of the patient until the cross-mark representing the projected tip and the predetermined entry point represented by the big aiming cross coincide. Guiding arrows indicate the direction and distance the tip of the instrument has to be moved about the skin

surface. The third dimension is easily assessed by maintaining the needle in contact with the skin. Two depth indicators provide additional help.

Needle alignment: Once the predetermined entry point has been found, the instrument is aligned with the planned trajectory. For this purpose, the *end* of the instrument, represented by a circle, is projected onto a plane orthogonal to the line connecting the tip of the instrument with the target point. The instrument can be pivoted around the contact point between its tip portion and the skin without losing the entry point until the circle has been moved to the center of the big aiming cross.

Needle insertion: In the last step, the needle is inserted into the tissue. For this purpose, a "virtual camera" is placed into the tip of the instrument with the view direction along the axis of the instrument. The trajectory is represented by a transparent tube, and a cross in the middle of the window helps aiming at the target point. The position of the tip of the instrument within the tube is indicated by a polygon-shaped structure. When the tip of the needle approaches the target point, the outer polygon (i.e., the end of the *surgery tube*) and the inner polygon approach each other, and the outer polygon touches the inner polygon just when the predetermined insertion depth is reached. This allows the user to focus the attention on the target point and the depth indication at the same time.

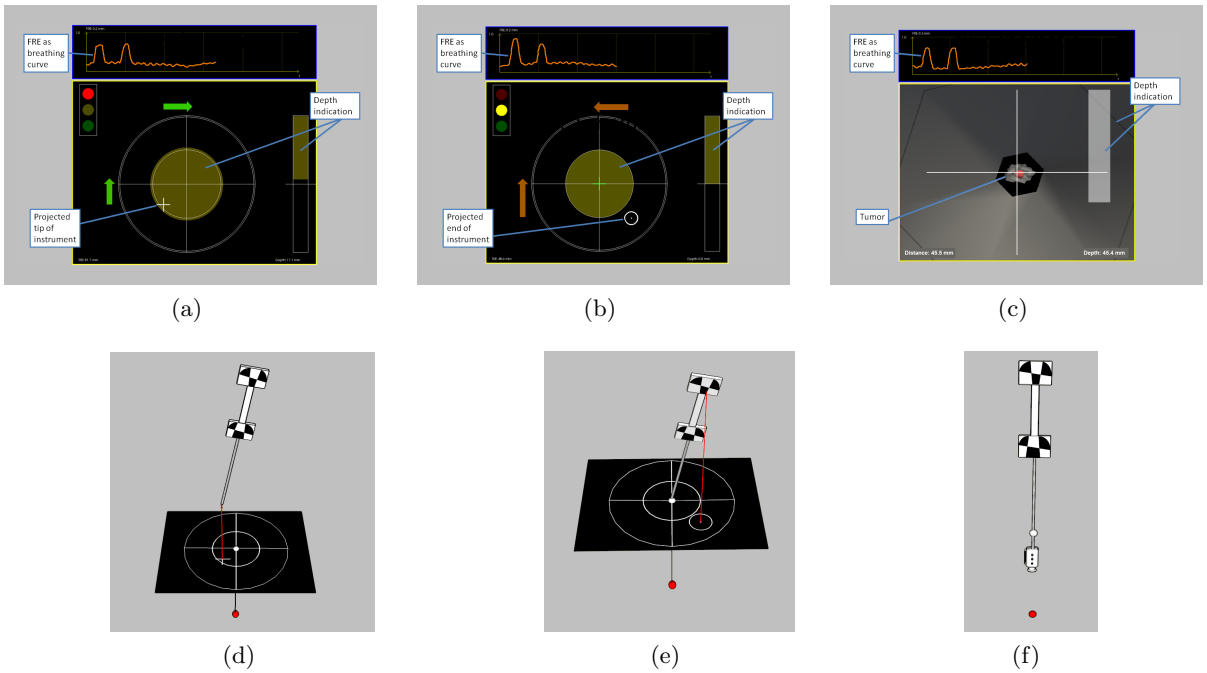

Figure 3. Three-stage visualization scheme providing separate views for the steps *tip positioning* (a), *needle alignment* (b), and *needle insertion* (c). In the corresponding schematic views (d,e,f), the planned trajectory is represented by a white insertion point and a red target point.

2.2 Robopsy system

The medical robot used for this study is the Robopsy system; a telerobotic, needle guidance and insertion system for CT-guided percutaneous interventions that has been described in detail in a previous report.[19] It consists of a lightweight, patient-mounted CT compliant robot device that can grip, orient and insert a needle or probe into the body. The current device is a prototype made using silicon molded plastic parts, and clearances on the order of 1 mm between parts are present. In a production molded device, the clearances would be sub-mm. The system was designed to be controlled by a point-and-click user interface that enables a radiologist to carry out the biopsy insertion from the radiation shielded control room. Figure 4(a) shows a schematic view of the robot device.

In this study, the robot will not be controlled by its point-and-click interface[20] but is integrated into the needle-based navigation system discussed in section 2.1. The needle is gripped by the robot and the optical tracking system (as opposed to CT scans) is used to provide feedback as to the needle position. The software then calculates the commands to be sent to the robot so as to align the needle along the desired trajectory and insert it to the appropriate depth.

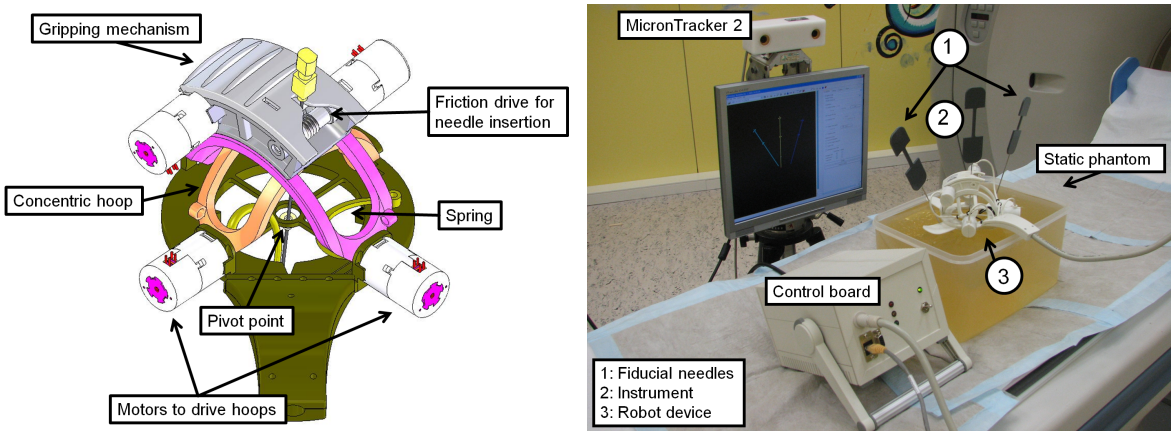

(a) (b)

Figure 4. Robopsy system: Schematic view of the robot device (a) and robotic-assisted targeting in the static phantom (b).

2.3 Phantoms

Two phantoms were applied in this study: a static abdominal phantom for assessing the operator error in a static environment and a motion simulator to assess the error *in-vitro*.

Static phantom: The static abdominal phantom is shown in Fig. 4(b). Is is comprised of ballistic gelatin, which has a consistency similar to human tissue and is used for ordnance testing (Vyse Gelatin Company, Schiller Park, IL, USA).

Motion simulator: The motion simulator was described in detail in a previous report.[21] A schematic representation is shown in Fig. 5. To use the device, it is necessary to mount an explanted human or porcine liver to the artificial diaphragm (Fig. 6(a)). Next, the simulator is connected to a lung ventilator whose settings control the breathing pattern. When the breathing bags are filled with air, the resulting force acting on the diaphragm model causes a movement of the diaphragm and thus of the liver in craniocaudal direction. When the lungs relax, elastic bands connected to the plate via two cylinders pull the diaphragm and therewith the liver back to its original position. Optionally, a ribcage with skin can be mounted to the patient model.

2.4 Experiments

To evaluate whether the operator error could be reduced by replacing the user with Robopsy, a set of targeting experiments were performed in the two phantoms introduced in section 2.3. The MicronTracker 2, model H40 (Claron Technology, Inc.; Toronto, Ontario, Canada), was applied for tracking the instrument to be inserted, and a set of (virtual) targets was defined in tracking coordinates. The navigation system introduced in section 2.1 was used to continuously compute the target position relative to the instrument. This approach allowed for isolation of the operator error from other error sources such as the localization of the instrument in a CT scan.

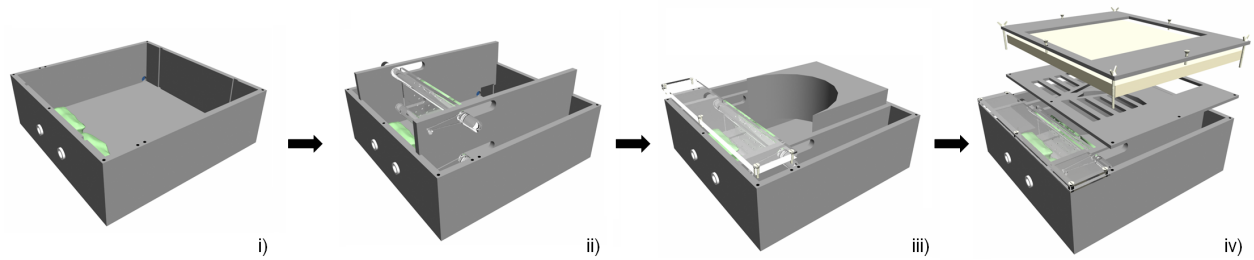

Figure 5. Schematic view of individual components of the respiratory liver motion simulator. i) Box with breathing bags and connections to lung ventilator. ii) Artificial diaphragm and construction for controlling respiratory motion. iii) Lung cover and filling element. iv) Ribcage with skin. For a clearer illustration, some of the modules are not shown in their original material (Plexiglas).

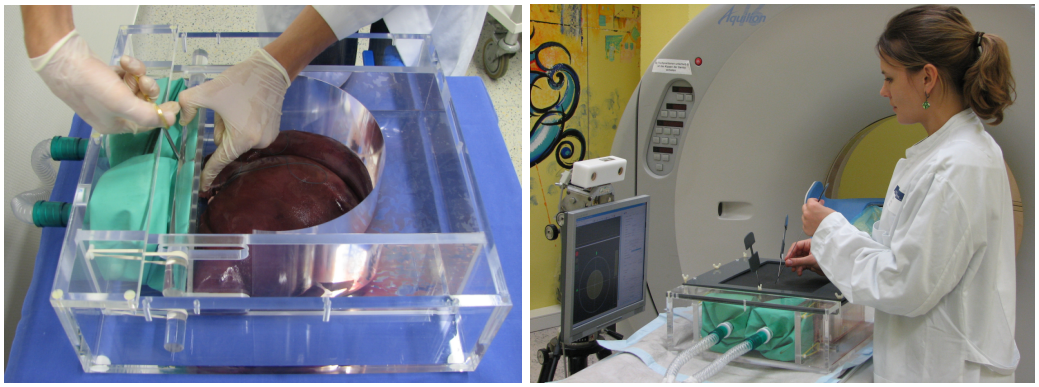

(a) (b)

Figure 6. Mounting of a porcine liver to the motion simulator (a) and computer-assisted needle insertion in the motion simulator (b).

2.4.1 Static experiments

For the experiments without target motion, a total of $n = 60$ needle insertions (*trials*) were performed in the abdominal phantom introduced in section 2.3 (30 trials with each method). The navigated placement was conducted by three different operators with experience with the navigation system (10 trials each). The remaining 30 punctures were performed by the robot operated by an engineer who was familiar with the device.

The workflow for each human operator was as follows:

1. Initially, two navigation aids were inserted into the phantom along the craniocaudal axis (cf. Fig. 6(b)).
2. The operator chose an insertion point between the two fiducial needles on the surface of the phantom by pointing at it with the tip of the tracked instrument.
3. The instrument was held perpendicular to the phantom surface, and 10 targets were computed on the sphere defined by the chosen insertion point and a radius (i.e., an insertion depth) of 7 cm. The insertion angles relative to the skin (i.e., to the surface of the phantom) were 0° (one target), 6° (three targets), 12° (three targets), and 18° (three targets).
4. For each target, the following workflow was performed:

   Tip positioning: Guided by the navigation monitor, the operator placed the tip of the tracked instrument onto the planned insertion point.

Needle alignment: Once the insertion point had been reached, the trajectory was continuously (re-) defined as the line connecting the tip of the instrument with the (virtual) target. The operator used the guidance monitor provided by the navigation system to align the instrument with the planned trajectory. When the operator confirmed completion of the subtask *needle alignment*, the angle between the axis of the instrument and the line connecting the target point with the tip of the instrument was recorded as alignment accuracy.

Needle insertion: The operator inserted the instrument towards the target. Once satisfied with the targeting accuracy, the operator confirmed completion of the subtask, and the distance of the tip of the instrument to the target was recorded as targeting error.

Needle releasing: The needle was released, and the distance of the of the instrument to the target was recorded again.

Correction: In order to determine if targeting errors that resulted after needle release could be corrected for, the human operator was allowed to correct for a perceived error from the guidance interface by re-gripping the needle and adjusting the insertion depth. After finally releasing the needle, accuracy was recorded again.

The time required for each of the subtasks was also recorded.

Similarly, the robot was used to perform a set of 30 targeting experiments. For each *pass* (ten targets), the robotic-assisted needle insertion workflow was as follows:

1. Initially, the robot was affixed to the phantom, and two navigation aids were inserted into the phantom along the craniocaudal axis (cf. Fig. 4(b)).

2. To establish a relationship between the tracking coordinate system and the robot coordinate system, the following calibration step was performed: The tracked instrument was used to target eight cone-shaped holes drilled into the base of the robot (with known positions in the robot coordinate system). Next, a rigid transformation was computed based on the least square method by Horn[22] to register the robot with the tracking coordinate system.

3. The insertion point was defined by the position of the robot, and 10 targets were defined relative to the insertion point as described above (workflow for human operators).

4. For each target, the following workflow was conducted:

   Tip positioning: The needle was gripped by the robot.

   Needle alignment: The planned trajectory was continuously (re-) defined as the line connecting the current tip position with the (virtual) target. The current needle pose and the planned trajectory were transformed to robot coordinates, and the robot was commanded to align the needle with the planned path. This step was repeated until no more improvements were obtained, i.e., the angle between the needle and the trajectory could not be decreased further. The angle between the axis of the instrument and the line connecting the target point with the tip of the instrument was then recorded as alignment accuracy.

   Needle insertion: The robot was commanded to insert the instrument towards the target based on the previously aligned trajectory, i.e., potential deviations in the alignment during insertion were not compensated for via optical feedback. This step was repeated until no more improvements (in terms of insertion depth) were made. The distance of the tip of the instrument to the target was then recorded as targeting error.

   Needle releasing: Finally, the needle was released, and the accuracy was recorded again.

   The time required for each of the subtasks was also recorded.

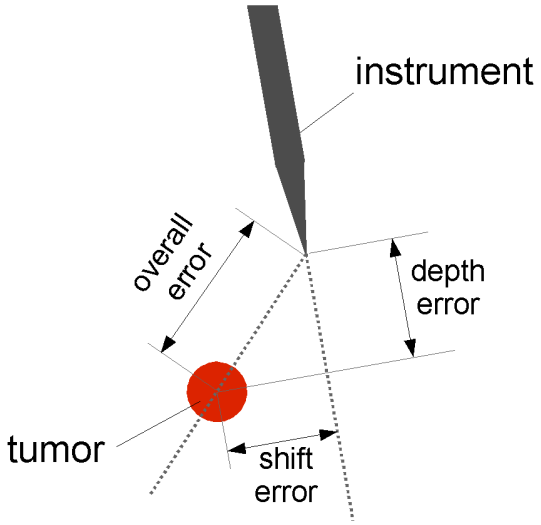

Figure 7. Illustration of the overall targeting error, the shift error, and the depth error.

For each targeting trial with the robot, the location of the needle and path was continuously recorded at a rate of 10 Hz so that any deviations of the needle from its desired trajectory after alignment could be detected.

In all experiments, the overall targeting error was subdivided into the *depth error* and the *shift error* as illustrated in Fig. 7.

2.4.2 *In-vitro* experiments

The experiment described in the previous section was then repeated in a porcine liver mounted to the motion simulator introduced in section 2.3. This time, only one human operator conducted the targeting experiments, i.e., a total of 20 needle insertions were performed *in-vitro* (10 with each method). The individual steps within the workflow were performed in full expiration. However, to account for respiratory motion, the simulator was activated for two breathing cycles between the steps *needle alignment* and *needle insertion*. This required minor re-alignment immediately prior to needle insertion.

3. RESULTS

The results of our study are shown in Tab. 1 and Fig. 8. In the static experiments, the accuracy of needle alignment was $0.2 \pm 0.1°$ (n = 30) for the robot and $0.6 \pm 0.2°$ (n = 30) for the human operators guided by the navigation system. There was no significant difference in the performance of the individual human operators. In the *in-vitro* liver experiments, the accuracy of needle alignment was $0.1 \pm 0.1°$ (n = 10) for the robot and $0.3 \pm 0.1°$ (n = 10) for the single human operator. According to Tab. 1, the overall targeting error for both sets of experiments was better for the human operators, yet, the depth error was better in the case of the robot as shown in Fig. 8.

The mean time required for *needle alignment* was 5 ± 1 s (static) and 8 ± 2 s (*in-vitro*) for the human operators and 24 ± 10 s (static) and 45 ± 16 s (*in-vitro*) in the case of the robot. Mean duration of *needle insertion* was 15 ± 3 s (static) and 20 ± 3 s (*in-vitro*) for the human operators while the robot achieved 42 ± 3 s (static) and 56 ± 16 s (*in-vitro*) on average. Correction of the needle position after release by the human operators took 12 ± 10 s (static) and 20 ± 7 s (*in-vitro*) on average.

In all experiments, the needle self-retracted slightly on release after insertion and this effect was more pronounced for the *in-vitro* experiments. This movement of the needle was considerably larger when the needle was inserted by the human operators (cf. Fig. 8). We found that by allowing them to re-grip the needle and insert it slightly after the initial insertion they were able to reduce this error with final mean targeting errors of 0.9 ± 0.4 mm and of 1.8 ± 0.8 mm for the static experiments and the *in-vitro* trials respectively.

(a) static accuracy

	S1	S2	S3	S1-S3	robot
alignment error [°]					
prior to insertion	0.6 ± 0.3	0.6 ± 0.2	0.6 ± 0.2	0.6 ± 0.2	0.2 ± 0.1
targeting error [mm]					
after insertion	0.8 ± 0.3	0.6 ± 0.2	0.8 ± 0.4	0.7 ± 0.3	2.3 ± 1.3
after release	1.6 ± 1.4	1.0 ± 0.5	1.0 ± 0.4	1.2 ± 0.9	2.2 ± 1.3
after correction	0.9 ± 0.3	0.7 ± 0.4	1.1 ± 0.6	0.9 ± 0.4	-

(b) *in-vitro* accuracy

	human	robot
alignment error [°]		
prior to insertion	0.3 ± 0.1	0.1 ± 0.1
targeting error [mm]		
after insertion	0.7 ± 0.3	1.8 ± 1.0
after release	5.5 ± 1.0	4.3 ± 1.6
after correction	1.8 ± 0.8	-

Table 1. Targeting accuracy for the experiments in the static phantom for the individual human operators (S1,S2,S3; n = 10 each), all human operators (S1-S3; n = 30) and the robot (n = 30) (a) and for the experiments in the motion simulator for the human operator (S1) (n = 10) and the robot (n = 10) (b).

4. DISCUSSION

This study investigated integration of the medical robot Robopsy into an existing needle-based navigation system for percutaneous interventions in the liver. For this purpose, navigated needle insertions were performed both in a static phantom and in a respiratory liver motion simulator, and the human operator error was compared with the error achieved by the medical robot. According to the results of this study, the robot performed a more accurate alignment of the instrument with the planned trajectory, achieving an angular error of the order of magnitude of 0.1 - 0.2° both in a static phantom and *in-vitro*. The insertion depth was also highly accurate, with an average error of 0.01 - 0.02 mm, while the human operators obtained depth errors of the order of magnitude of 0.1 - 0.2 mm.

With such an accurate alignment and insertion capability one would expect the overall targeting error (i.e., the distance between the needle tip and the virtual target after insertion) to be better for the robot; however, in this initial study we found this not to be the case. We believe that a large portion of the error can be explained by a slight miscalibration of the axis of the tracked instrument. The effect of this would be to lead to a shift error after needle insertion as illustrated in Fig. 9. During the experiments, the needle was observed to rotate about its own axis during insertion, likely as a result of a slight misalignment of the needle due to gravity when gripped by the rollers. Unlike the robot, the human operators, who did not rotate the needle during insertion, were not as affected by this miscalibration and so achieved a better shift error.

Another possible explanation for the larger shift for the robot was that the robot used for these experiments was rapid prototyped using silicon molds, and thus, the plastic parts did not have the close tolerances that a production version would have. In consequence, a reaction force on the carriage and the hoops during needle insertion may have resulted in a slight deflection of the carriage. However, careful analysis of the continuous positional data recorded during instrument insertion showed that only small changes of the vector defining the axis of the needle in robot coordinates were observed during insertion. These small changes were not sufficient to explain the shift error but may have contributed to it. In the current implementation of the robot control software, no feedback from the tracking system was used to command the robot to update the needle angle during insertion, and so this error could not be removed. In contrast, the human operators were able to perform minor corrections of the angle of the instrument during insertion - at least in the phantom when the tissue provided less resistance to needle movement.

While there was only a slight self-retraction of the needle after releasing it in the case of the gelatin phantom, this effect was considerable after release in the case of the *in-vitro* liver experiments. This can be attributed to

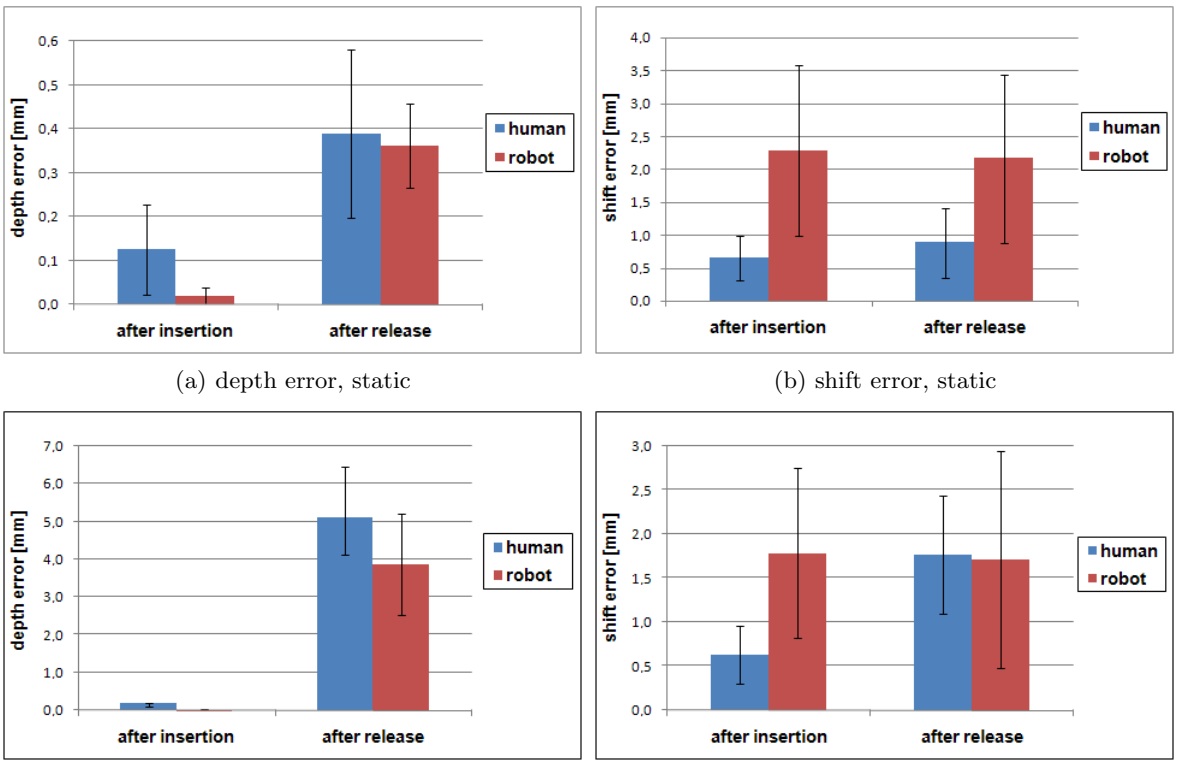

(a) depth error, static

(b) shift error, static

(c) depth error, *in-vitro*

(d) shift error, *in-vitro*

Figure 8. Depth error and shift error according to Fig. 7 in the gelatin phantom (a,b) and in the motion simulator (c,d) after needle insertion and after releasing the needle.

the following factors. First, the instrument was not anchored within the tissue after insertion. Consequently, the elastic skin potentially pulled the needle a couple of millimeters out of the liver upon release. Second, the instrument was re-used many times and thus possibly not sharp enough, which may have led to local deformation of the liver that was not captured by the fiducial needles. Finally, although a relatively big needle diameter of 2 mm was chosen, the user may have bent the instrument during insertion which then resulted in the needle angle changing after release and thus causing a shift error. Interestingly, the instrument shift after release was considerably bigger in the case of the human operators. We attribute this to the fact that the human operator tried to correct for alignment errors during instrument insertion and that when the needle was released, the elastic liver tissue pulled it back, causing the needle to unbend and resulting in a shift error (cf. Fig. 8(d)).

Literature on robotic-assisted needle insertion into soft tissue is relatively sparse. A general review of robotic systems for image-guided interventions can be found in.[23,24] The systems presented for minimally-invasive needle insertion into abdominal organs include those introduced by Su *et al.*,[25] Kim *et al.*,[26] Kettenbach *et al.*[27] and Maurin *et al.*[28] Several papers have been published on the accuracy of medical robots[27–29] as well as on the comparison between conventional and robotic-assisted medical interventions,[25,30] yet, integration of a medical robot with an existing soft tissue navigation system to reduce the operator error has - to our knowledge - not yet been investigated.

Based on our initial experience of integrating the robot with the navigation system presented in this study, the Robopsy driven needle insertion system is able to more accurately align the needle and insert it along its axis compared to the human operator. This was to be expected and is a known advantage of robotic systems that have high positioning resolution. With such high angular and insertion accuracy we expect the combined navigation and robotic system to be able to place the needle more accurately and precisely than an operator with the navigation system alone. However, in this initial study we found that this was not the case, most probably due to the shift error caused by a miscalibrated axis of the instrument as discussed above and some slight play

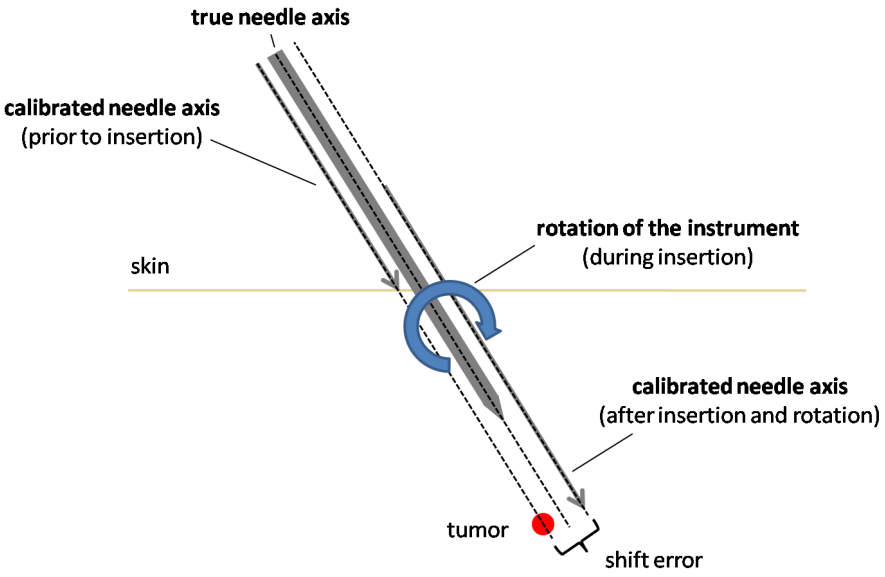

Figure 9. Illustration of the effect of a miscalibrated instrument onto the operator error, when the needle rotates about its own axis during insertion.

in the mechanical parts due to the device being a prototype.

A major advantage of the robot is that it is attached to the patient and so any sudden movements of the patient are compensated for passively as the device moves with the patient. Also, it does not require physical presence of the operator in the CT room and can be used to stabilize the instrument during CT scan acquisition even if it is not inserted deeply into the liver. However, additional hardware is required for the robot which adds cost, and so it is important that the robot must be designed to be cost effective in order to improve overall procedural efficiency. Another point is that the robot restricts the maximum angulation of the needle to $\pm 30^\circ$ from the center of the device; however, discussions with radiologists reveal that this is adequate for most procedures as it is desirable for needle entry to be perpendicular to the skin.

The comparison between the two systems also provides insights into how the control software of the robot can be modified. For example, when the needle was released after initial insertion, the user re-gripped and inserted it a small amount more and was thus able to achieve a lower targeting error - something we also observed in previous animal studies with the navigation system alone.[16] We plan to modify the system to include these features in the operation of the robot so as to achieve an improved targeting error.

In conclusion, integration of Robopsy into the existing navigation system is likely to lead to a lower operator and thus overall targeting error in the future. The hardware and software of the robot is currently being modified to allow for a faster insertion speed. Furthermore, better integration of the robot with the navigation system and a reduction of the play between the plastic parts in the robot through tighter part tolerances in a production version will further improve the performance of the system. Once optimized, the combined system will be evaluated in a clinical setting.

5. ACKNOWLEDGEMENTS

The present study was conducted within the setting of "Research training group 1126: Intelligent Surgery - Development of new computer-based methods for the future workplace in surgery" funded by the German Research Foundation (DFG).

The authors would like to thank Thomas Roschke, Joerg Gassmann and Patrick Anders from Saia-Burgess Dresden GmbH (a Johnson Electric company) for their assistance with the development of the Robopsy prototype

as well as the Center for Integration of Medicine and Innovative Technology (CIMIT) for providing the funding for the Robopsy project.

REFERENCES

[1] Grant, A. and Neuberger, J., "Guidelines on the use of liver biopsy in clinical practice," *Gut* **45**, IV1–IV11 (1999).

[2] Clifford, M. A., Banovac, F., Levy, E., and Cleary, K., "Assessment of hepatic motion secondary to respiration for computer assisted interventions," *Comp Aid Surg* **7**, 291–299 (2002).

[3] Pereira, P. L., "Actual role of radiofrequency ablation of liver metastases," *Eur Radiol* **17**(8), 2062–2070 (2007).

[4] Rhim, H., Goldberg, S. N., Dodd, G. D., Solbiati, L., Lim, H. K., Tonolini, M., and Cho, O. K., "Essential techniques for successful radio-frequency thermal ablation of malignant hepatic tumors," *Radiographics* **21**, 17–35 (2001).

[5] Nagel, M., Schmidt, G., Petzold, R., and Kalender, W. A., "A navigation system for minimally invasive CT-guided interventions," in [*Medical Image Computing and Computer-Assisted Intervention - MICCAI 2005 (2)*], Duncan, J. S. and Gerig, G., eds., 33–40, Springer, Palm Springs, Ca, USA (2005).

[6] Fichtinger, G., Deguet, A., Fischer, G., Iordachita, I., Balogh, E., Masamune, K., Taylor, R. H., Fayad, L. M., de Oliveira, M., and Zinreich, S. J., "Image overlay for CT-guided needle insertions," *Comp Aid Surg* **10**(4), 241–255 (2005).

[7] Khan, M. F., Dogan, S., Maataoui, A., Wesarg, S., Gurung, J., Ackermann, H., Schiemann, M., Wimmer-Greinecker, G., and Vogl, T. J., "Navigation-based needle puncture of a cadaver using a hybrid tracking navigational system," *Invest Radiol* **41**(10), 713–720 (2006).

[8] Das, M., Sauer, F., Schoepf, U. J., Khamene, A., Vogt, S. K., Schaller, S., Kikinis, R., vanSonnenberg, E., and Silverman, S. G., "Augmented reality visualization for CT-guided interventions: System description, feasibility, and initial evaluation in an abdominal phantom," *Radiology* **240**(1), 230–235 (2006).

[9] Wacker, F. K., Vogt, S., Khamene, A., Jesberger, J. A., Nour, S. G., Elgort, D. R., Sauer, F., Duerk, J. L., and Lewin, J. S., "An augmented reality system for MR image-guided needle biopsy: Initial results in a swine model," *Radiology* **238**(2), 497–504 (2006).

[10] Wallace, M. J., Gupta, S., and Hicks, M. E., "Out-of-plane computed-tomography-guided biopsy using a magnetic-field-based navigation system," *Cardiovasc Inter Rad* **29**, 108–113 (2006).

[11] Zhang, H., Banovac, F., Lin, R., Glossop, N., Wood, B. J., Lindisch, D., Levy, E., and Cleary, K., "Electromagnetic tracking for abdominal interventions in computer aided surgery," *Comp Aid Surg* **11**(3), 127–36 (2006).

[12] Nicolau, S. A., Pennec, X., Soler, L., and Ayache, N., "Clinical evaluation of a respiratory gated guidance system for liver punctures," in [*Medical Image Computing and Computer-Assisted Intervention - MICCAI 2007 (2)*], Ayache, N. and et al., eds., **4792**, 77–85, Springer, Brisbane, Australia (October 2007).

[13] Krücker, J., Xu, S., Glossop, N., Viswanathan, A., Borgert, J., Schulz, H., and Wood, B. J., "Electromagnetic tracking for thermal ablation and biopsy guidance: clinical evaluation of spatial accuracy," *J Vasc Interv Radiol* **18**(9), 1141–50 (2007).

[14] Maier-Hein, L., Pianka, F., Seitel, A., Müller, S. A., Tekbas, A., Seitel, M., Wolf, I., Schmied, B. M., and Meinzer, H.-P., "Precision targeting of liver lesions with a needle-based soft tissue navigation system," in [*Medical Image Computing and Computer-Assisted Intervention - MICCAI 2007 (2)*], Ayache, N., Ourselin, S., and Maeder, A., eds., **4792**, 42–49, Springer, Brisbane, Australia (October 2007).

[15] Maier-Hein, L., Müller, S. A., Pianka, F., Wörz, S., Müller-Stich, B. P., Seitel, A., Rohr, K., Meinzer, H.-P., Schmied, B. M., and Wolf, I., "Respiratory motion compensation for CT-guided interventions in the liver," *Comp Aid Surg* **13**(3), 125–38 (2008).

[16] Maier-Hein, L., Tekbas, A., Seitel, A., Pianka, F., Müller, S. A., Satzl, S., Schawo, S., Radeleff, B., Tetzlaff, R., Franz, A. M., Müller-Stich, B. P., Wolf, I., Kauczor, H.-U., Schmied, B. M., and Meinzer, H.-P., "In-vivo accuracy assessment of a needle-based navigation system for ct-guided radiofrequency ablation of the liver," *Med Phys* **35**(12), 5385–5396 (2008).

[17] Maier-Hein, L., Tekbas, A., Franz, A. M., Tetzlaff, R., Müller, S. A., Pianka, F., Wolf, I., Kauczor, H.-U., Schmied, B. M., and Meinzer, H.-P., "On combining internal and external fiducials for liver motion compensation," *Comp Aid Surg* **13**(16), 369–376 (2008).

[18] Wolf, I., Vetter, M., Wegner, I., Böttger, T., Nolden, M., Schöbinger, M., Hastenteufel, M., Kunert, T., and Meinzer, H.-P., "The medical imaging interaction toolkit," *Medical Image Anal* **9**(6), 594–604 (2005).

[19] Walsh, C. J., Hanumara, N. C., Slocum, A. H., Shepard, J.-A., and Gupta, R., "A patient-mounted, telerobotic tool for CT-guided percutaneous interventions," *J Med Devices* **2**, 011007 (10 pages) (March 2008).

[20] Seitel, A., Walsh, C. J., Hanumara, N. C., Shepard, J. O., Slocum, A. H., Meinzer, H.-P., Gupta, R., and Maier-Hein, L., "Development and evaluation of a new image-based user interface for robot-assisted needle placements with the robopsy system," in [*SPIE Medical Imaging 2009: Visualization, Image-guided Procedures and Modeling*], Miga, M. I. and Wong, K. H., eds. (2009). (to appear).

[21] Maier-Hein, L., Pianka, F., Müller, S. A., Rietdorf, U., Seitel, A., Franz, A. M., Wolf, I., Schmied, B., and Meinzer, H.-P., "Respiratory liver motion simulator for validating image-guided systems ex-vivo," *Int J CARS* **2**(5), 287–92 (2008).

[22] Horn, B., "Closed-form solution of absolute orientation using unit quaternions," *J Opt Soc Am A* **4**, 629–642 (1987).

[23] Pott, P. P., Scharf, H.-P., and Schwarz, M. L. R., "Today's state of the art in surgical robotics," *Comp Aid Surg* **10**, 101–132 (March 2005).

[24] Cleary, K., Melzer, A., Watson, V., Kronreif, G., and Stoianovici, D., "Interventional robotic systems: Applications and technology state-of-the-art," *Minim Invasive Ther Allied Technol* **15**, 101–113 (April 2006).

[25] Su, L. M., Stoianovici, D., Jarrett, T. W., Patriciu, A., Roberts, W. W., Cadeddu, J. A., Ramakumar, S., Solomon, S. B., and Kavoussi, L. R., "Robotic percutaneous access to the kidney: comparison with standard manual access," *J Endourol* **16**(7), 471–475 (2002).

[26] Kim, D., Kobayashi, E., Dohi, T., and Sakuma, I., "A new, compact MR-compatible surgical manipulator for minimally invasive liver surgery," in [*Medical Image Computing and Computer-Assisted Intervention MICCAI 2002*], 164–169 (2002).

[27] Kettenbach, J., Kronreif, G., Figl, M., Fürst, M., Birkfellner, W., Hanel, R., and Bergmann, H., "Robot-assisted biopsy using ultrasound guidance: initial results from in vitro tests," *Eur Radiol* **15**(4), 765–771 (2005).

[28] Maurin, B., Bayle, B., Piccin, O., Gangloff, J., de Mathelin, M., Doignon, C., Zanne, P., and Gangi, A., "A patient-mounted robotic platform for CT-scan guided procedures," *IEEE T Bio-Med Eng* **55**(10), 2417–2425 (2008).

[29] Stoianovici, D., Cleary, K., Patriciu, A., Mazilu, D., Stanimir, A., Craciunoiu, N., Watson, V., and Kavoussi, L., "AcuBot: a robot for radiological interventions," *IEEE T Robotic Autom* **19**(5), 927 – 930 (2003).

[30] Ma, G. W., Pytel, M., Trejos, A. L., Hornblower, V., Smallwood, J., Patel, R., Fenster, A., and Malthaner, R. A., "Robot-assisted thoracoscopic brachytherapy for lung cancer: comparison of the zeus robot, vats, and manual seed implantation," *Comp Aid Surg* **12**(5), 270–277 (2007).